

Picosecond Multiphoton Scanning Near-Field Optical Microscopy

Attila Jenei, Achim K. Kirsch, Vinod Subramaniam, Donna J. Arndt-Jovin, and Thomas M. Jovin

Department of Molecular Biology, Max Planck Institute for Biophysical Chemistry, Am Fassberg 11, D-37077 Göttingen, Germany

ABSTRACT We have implemented simultaneous picosecond pulsed two- and three-photon excitation of near-UV and visible absorbing fluorophores in a scanning near-field optical microscope (SNOM). The 1064-nm emission from a pulsed Nd:YVO₄ laser was used to excite the visible mitochondrial specific dye MitoTracker Orange CM-H₂TMRos or a Cy3-labeled antibody by two-photon excitation, and the UV absorbing DNA dyes DAPI and the bisbenzimidazole BBI-342 by three-photon excitation, in a shared aperture SNOM using uncoated fiber tips. Both organelles in human breast adenocarcinoma cells (MCF 7) and specific protein bands on polytene chromosomes of *Drosophila melanogaster* doubly labeled with a UV and visible dye were readily imaged without photodamage to the specimens. The fluorescence intensities showed the expected nonlinear dependence on the excitation power over the range of 5–40 mW. An analysis of the dependence of fluorescence intensity on the tip-sample displacement normal to the sample surface revealed a higher-order function for the two-photon excitation compared to the one-photon mode. In addition, the sample photobleaching patterns corresponding to one- and two-photon modes revealed a greater lateral confinement of the excitation in the two-photon case. Thus, as in optical microscopy, two-photon excitation in SNOM is confined to a smaller volume.

INTRODUCTION

Fluorescence microscopy is arguably the most powerful experimental technique for visualization of biological specimens. Fluorescent small molecule probes or luminescent proteins can be attached to specific molecules targeted to particular cell organelles both *in vivo* and *in vitro* (Gerdes and Kaether, 1996; Haugland, 1996). These probes indicate the distribution or morphology of their target structures and also report on the properties of the local environment. The large span of the emission spectra of these probes, ranging from the near-UV to the near-IR region of the electromagnetic spectrum, allows the simultaneous detection and discrimination of multiple fluorescent markers. In conventional laser fluorescence microscopy, the use of fluorophores absorbing and emitting in the near-UV poses several practical problems, e.g., the high cost of UV laser systems, requirement for high quality UV optics, and significant chromatic aberration. However, the introduction in microscopy (Denk et al., 1990) and subsequent widespread application of molecular two-photon excitation (2PE), in which a molecule absorbs two photons in a single quantum event, a phenomenon predicted by Maria Göppert-Mayer in 1931 (Göppert-Mayer, 1931), has overcome these problems. Three-photon excited (3PE) fluorescence spectroscopy and microscopy has also been demonstrated (Gryczynski et al., 1995; Hell et al., 1996; Szmajcinski et al., 1996; Maiti et al., 1997). These modes enable excitation of near-UV fluorophores with visible or IR light, and enhance

the performance of traditional microscopes because of reduced scattering of the longer wavelength photons, increased depth penetration of thick samples, and reduced autofluorescence, photobleaching, and phototoxic effects on living organisms resulting from the limitation of excitation to a small volume around the focus. The emission induced by nonlinear excitation is indistinguishable from that in single-photon excitation (Curley et al., 1992; Xu and Webb, 1996). In addition, multiphoton excitation leads to a lower background and higher signal-to-noise ratio because the excitation light is spectrally widely separated from the resulting fluorescence emission, and thus can be suppressed much more efficiently. For all of the above reasons, 2PE and 3PE are finding multiple applications in laser scanning and high-resolution microscopy (Denk et al., 1990, 1995; Bennett et al., 1996; Hell et al., 1996, 1998; König et al., 1996; Potter et al., 1996; Summers et al., 1996; Wokosin et al., 1996; Bewersdorf and Hell, 1998), thereby extending the useful range of laser-induced fluorescence microscopy.

The signal of 2PE and 3PE fluorophores is proportional to the time-averaged square and cube, respectively, of the excitation light intensity, and is thus enhanced by the use of repetitive short laser pulses. For lasers emitting pulses of length τ at a repetition rate f , the increase of the 2PE fluorescence signal relative to a cw source with the same average power is $\sim 1/(\tau \cdot f)$ (Denk et al., 1995). In 3PE, the corresponding factor scales as $\sim 1/(\tau \cdot f)^2$ (Xu et al., 1996; Schrader et al., 1997). The 2PE boost factor value can be $5 \cdot 10^4$ ($\tau = 250$ fs, $f = 80$ MHz) for a typical femtosecond Ti:sapphire laser system, and has led to the general use of fs-laser systems in multiphoton laser scanning microscopy (Denk et al., 1990; Wokosin et al., 1996). Unfortunately, such systems are technically complex and expensive. A compromise between such fs Ti:sapphire systems and 2PE based on cw laser systems of higher average power, but consequently limited sample stability (Hänninen et al.,

Received for publication 24 August 1998 and in final form 30 October 1998.

Address reprint requests to Dr. Thomas M. Jovin, Department of Molecular Biology, Max Planck Institute for Biophysical Chemistry, Am Fassberg 11, D-37077 Göttingen, Germany. Tel.: +49-551-201-1381; Fax: +49-551-201-1467; E-mail: tjovin@mpc186.mpibpc.gwdg.de.

© 1999 by the Biophysical Society

0006-3495/99/02/1092/09 \$2.00

1994), is provided by solid state picosecond (ps) lasers. For a ps laser with $\tau = 7$ ps and 200 MHz (characteristic of the laser used in this study), the $1/\tau f$ boost factor is ~ 700 . In order to achieve signal levels in 2PE similar to those attained by fs-laser systems, the average power of the excitation in the ps case thus has to be increased by the modest factor of ~ 8 , resulting in average power levels of ~ 10 – 40 mW (Bewersdorf and Hell, 1998).

Near-field microscopes achieve resolution of surface structures beyond the diffraction limit of far-field microscopy by detecting the optical interaction between a small nanometer-sized probe and the sample surface (Paesler and van Hulst, 1995). In scanning near-field optical microscopy (SNOM) the fluorescence background signal is in general quite high due to the generation of fluorescence and Raman scattering in the optical fiber used to couple the scanning probe to macroscopic light sources and/or detectors. With 2PE the contribution of these sources to the detected signal are reduced because the emitted fluorescence occurs at higher energies, and therefore shorter wavelengths, than the excitation laser or the undesirable inelastic scattering processes. Femtosecond (fs)-pulsed (Lewis et al., 1998) and cw lasers (Kirsch et al., 1998b) have been shown to be viable two-photon excitation sources for SNOM, particularly in the shared aperture mode of operation (Kirsch et al., 1998b).

In our implementation of cw 2PE in SNOM for exciting near-UV absorbing fluorophores in biological systems (Kirsch et al., 1998b), a drawback was the limited stability of samples at the high (hundreds of milliwatts) average power levels required for achieving adequate signal levels.

Here we report the implementation of simultaneous ps-pulsed 2PE of dyes excitable in the visible green range and 3PE of near-UV absorbing fluorophores in a SNOM. We used a solid-state (Nd:YVO₄) ps laser operated at 1064 nm, and observed that efficient 3PE already occurred at moderate excitation power levels of ~ 40 mW. This combination of multiphoton excitation provides simultaneous dual color imaging without cross talk between the emission signals. Additionally, the use of a frequency-doubled cw Nd:YAG laser in the same configuration has allowed a direct comparison of the characteristics of single-photon excitation (1PE) and 2PE of the same sample.

MATERIALS AND METHODS

Dyes and antibodies

DAPI (4',6-diamidino-2-phenylindole) was purchased from Serva (Heidelberg, Germany), the bisbenzimidazole Hoechst 33342 (BBI-342) from Calbiochem (Bad Soden, Germany), MitoTracker Orange CM-H₂TMRos (M7511) from Molecular Probes (Leiden, the Netherlands), and rhodamine B from Merck (Darmstadt, Germany). Rabbit polyclonal antibody against the *Drosophila* protein polyhomeotic (PH) was raised in our laboratory and checked for specificity by Western blotting to embryo extracts and immunofluorescence on salivary gland polytene chromosome preparations. Secondary Cy3-conjugated goat-anti-rabbit (Fab)₂ antibody was purchased from Dianova (Hamburg, Germany).

Cell culture

Human breast adenocarcinoma (MCF7 ATCC HTB22) cells were maintained in Dulbecco's modified Eagle's medium (Life Sciences Technologies, Eggenstein, Germany) supplemented with 10% fetal calf serum and 2 mM L-glutamine at 37°C in a CO₂ incubator. For microscopy, cells were grown on glass coverslips (12 mm diameter).

Cell labeling and preparation

Cells, growing on coverslips, were labeled first with 0.5 μ M MitoTracker in complete medium for 30–60 min at 37°C, washed three times in phosphate buffered saline (PBS), and fixed for 10 min at room temperature in freshly prepared 3.7% paraformaldehyde in buffer followed by three washes in 25 mM Tris-HCl, pH 7.2, 120 mM NaCl. Cells were counterstained after fixation with 10 μ M BBI-342 for 15 min at room temperature. In some experiments the cell membranes were extracted after fixation in order to expose mitochondria by treatment with 0.2% Triton X-100 and 4 M glycerol in a stabilization buffer (Na-Pipes, pH 6.9, 0.5 mM MgCl₂, and 0.1 mM EDTA) for 3 min (Pietrasanta et al., 1994). Coverslips were rinsed twice with PBS and dehydrated through an ethanol series, air dried, and stored in a desiccator. In some experiments we applied hexamethyldisilazane (HMDS) (Sigma, Diesenhofen, Germany) after dehydration for stabilization of the cellular samples (Braet et al., 1997).

Polytene chromosomes

Polytene chromosomes were prepared from salivary glands of *Drosophila melanogaster* 3rd-instar larvae, fixed with paraformaldehyde, and squashed according to established protocols (Ashburner, 1989). The squashed chromosomes were washed in PBS and incubated with a polyclonal antibody against polyhomeotic, a protein of the Polycomb Group, for 2 h in PBS containing 0.02% Triton X-100 and 0.5 mg/ml BSA. Chromosomes were washed twice for 5 min with PBS, incubated with a Cy3 conjugated polyclonal goat anti-rabbit (Fab)₂ antibody (Cy3-GARIG) for 1 h, washed in PBS, and stained with 5 mM DAPI in PBS for 5 min. After rinsing twice with PBS, samples were exchanged into ethanol through a graded concentration series, air dried, and stored in a desiccator. In some cases the chromosomes were kept hydrated after staining and measured in the presence of a water film.

Dye-doped polyvinylalcohol films

Rhodamine B was dissolved to 10 μ M in a 1% polyvinylalcohol (PVA) solution. Films were formed by dipping freshly cleaved mica coverslips into the dye-PVA solution. Samples were air dried.

SNOM

Instrument

The SNOM used for the experiments comprises a shear force sensor head developed in our laboratory (Kirsch et al., 1997, 1998b) as an add-on to a Nanoscope-IIIa scanning probe system (Digital Instruments, Santa Barbara, CA). It uses uncoated fiber tips for both excitation and detection of the fluorescence (shared aperture mode) (Courjon et al., 1990; Bielefeldt et al., 1994; Kirsch et al., 1996). The tips were produced with a commercial pipette puller (P-2000, Sutter Instruments, Novato, CA) from a 9- μ m core diameter optical fiber (SMF 1528 CPC6, Siecor, Neustadt, Germany) and mounted in the sensor head. All measurements were performed under ambient conditions (relative humidity 45–60%, 18–24°C).

Lasers

The light source for multiphoton excitation (2PE, 3PE) was a pulsed diode-pumped Nd:yttrium-vanadate (Nd:YVO₄) laser with a repetition rate

of 200 MHz and a fixed pulse width of 7.1 ps (GE 100, Time Bandwidth Products, Zürich, Switzerland). The laser is passively mode-locked with a semiconductor saturable absorber mirror (SESAM) and emits at 1064 nm with an average power of ~200 mW. 1PE was accomplished with a 50 mW frequency-doubled, low-noise, cw Nd:YAG solid state laser operating at 532 nm (CGL-050-L CrystaLaser, Reno, NV).

Optical configuration

The optical configuration in multiphoton SNOM is shown in Fig. 1. Both lasers were combined with a dichroic (Dich. 1, HR1064, Jenoptik, Jena, Germany) and coupled simultaneously into the fiber. Alternating synchronized shutters were put in front of the lasers to switch between the light sources. For the quasi-simultaneous comparison of 1PE and 2PE we used a dichroic element reflective at 532 nm and 1064 nm (Dich. 2, HR532/1064, Jenoptik). In this experiment, the output from the 532-nm cw Nd:YAG laser was attenuated with neutral density filters (New Focus, Inc., Santa Clara, CA) to yield an emission signal comparable to that from the pulsed laser. For simultaneous 2PE and 3PE, a dichroic mirror with high transmission in the visible and reflection centered at 1064 nm (HR1064, Jenoptik) was placed at the position marked Dich. 2 in Fig. 1.

Fluorescence detection

The fluorescence of the 3PE UV-absorbing DNA probes DAPI and BBI-342 was separated from the emission of the 2PE MitoTracker, Cy3, and rhodamine B with a DCLP 565 dichroic mirror (Dich. 3, Chroma Technology, Brattleboro, VT) and filtered with a SWP 490 bandpass filter (Em. 3, Delta Light and Optics, Lyngby, Denmark). The fluorescence of the 2PE dyes was further filtered with a SWP 605/55 bandpass filter (Em. 2,

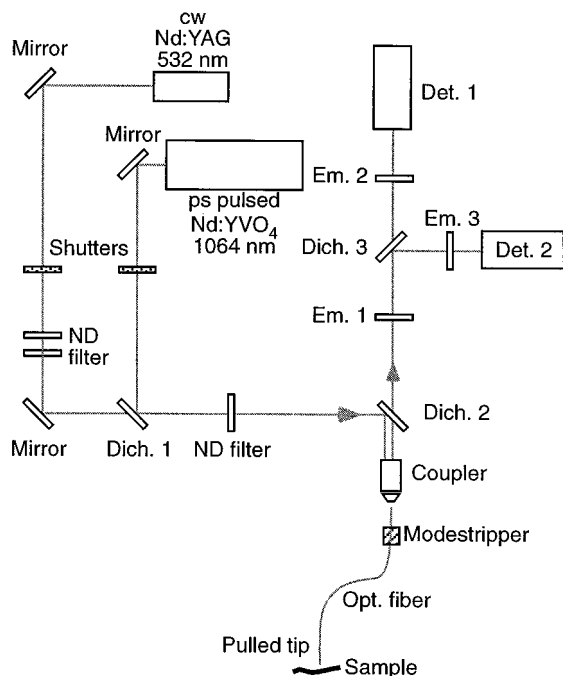


FIGURE 1 Optical configuration in multiphoton SNOM. During 1PE and 2PE measurements we alternated between the laser sources using shutters. The pulsed and cw lasers were coupled simultaneously into the fiber using dichroic mirrors (Dich. 1 and Dich. 2). A mode-stripper (see text for details) was used to suppress the cladding modes causing fiber fluorescence. A dichroic mirror (Dich. 3) was used to separate the 2PE and 3PE emission signals. Other abbreviations: Em, emission filters; ND, neutral density filters; Det, detector.

Chroma Technology, Brattleboro, VT). The residual IR excitation and the light from the shear force detection system were blocked by a combination of blue glass filters (Em. 1, 1 mm BG40, 2 mm BG39; Jenaer Glaswerk Schott and Gen., Mainz, Germany). The detectors (Det. 1 and Det. 2) were single photon-counting avalanche photodiodes (APDs, SPCM-AQ131 for 3PE and SPCM-AQ231 for 2PE, EG&G Optoelectronics, Canada). The TTL outputs were directed to the pulse counting boards of the nanoscope. Images were processed with the Nanoscope software.

Mode-stripper

In 1PE shared-aperture fluorescence measurements we often observed a high background signal primarily due to fluorescence of the protective polymer coating excited by cladding modes launched during the coupling of the excitation laser into the fiber. This background could be significantly reduced either by removing the entire coating from the fiber (thus rendering it much more susceptible to breakage) or by inserting a passive component (mode-stripper) after the coupler. In the mode-stripper, a short length of the bare glass fiber (stripped free of its coating) is immersed in an oil bath (~17 mm length) of higher refractive index ($n = 1.518$) than the fiber, allowing the cladding modes to escape from the fiber into the surrounding medium (Kirsch, 1998).

Power curves

Fluorescence power curves were measured by varying the excitation intensity using neutral density filter wheels (New Focus) and recording the fluorescence detected by the APD with an external photon counter (SR400, Stanford Research Systems, Sunnyvale, CA). All measurements were carried out with both increasing and decreasing excitation light levels measured at the end of the pulled tip. The photon counter and the shutters in front of the laser sources were under computer control, ensuring that the samples were illuminated only during the measurement. The fluorescence power curves for the stained samples were recorded with the tip in shear-force feedback and zero scan size.

Z-scans

Z-scans were performed by bringing the tip from ~3 μm above the sample surface into feedback control while recording the fluorescence. The z axis of the scan piezo was calibrated in a separate measurement against a piezo system with capacitive sensors and closed loop position control (P-730.20, Physik Instrumente, Waldbronn, Germany) (Kirsch et al., 1998b).

Photobleaching records

Photobleaching experiments were performed by repeatedly scanning a given line while continuously illuminating the sample. For postbleaching visualization, the scan direction was rotated by 90° and the scan area was increased twofold.

Data analysis procedure

Fluorescence-distance curves

Each experiment generated a number of approach curves with decreasing distance between probe and sample surface. In each approach curve n points (generally 160–400) were collected using single photon counting. As before, photobleaching reduced the fluorescence intensity in successive approaches. Assuming a constant distance dependence, all curves were fit simultaneously to a double exponential function with global decay lengths.

RESULTS AND DISCUSSION

2PE imaging of cells

A SNOM image of a MitoTracker-labeled MCF7 cell is depicted in Fig. 2. The shear force topography signal (*A*), topographic feedback (error) signal (*B*), and 2PE fluorescence signal from the labeled mitochondria (*C*) were collected simultaneously. The average height of the dried cells was ~ 800 nm, reflecting cytoplasmic collapse due to the drying procedure (Pietrasanta et al., 1994). The smooth, approximately circular domain with several high protrusions corresponded to the nuclei located within a highly structured cytoplasmic area. The protrusions rising 300 nm above the nucleus were the dense nucleoli, observed previously by SNOM in 3T3 Balb/c cells (Kirsch et al., 1998b). In the 2PE fluorescence signal (Fig. 2 *C*) the MitoTracker-labeled mitochondria were perceived as perinuclear structures. There was some faint accumulation of the dye in the nucleoli, also observed in conventional confocal microscopy (data not shown). The fluorescence of the region boxed in Fig. 2 *C* was recorded at higher magnification (Fig. 2 *D*). A cross-sectional average line-plot of the fluorescence from the area marked in Fig. 2 *D* is shown in Fig. 2 *E*. The smallest resolved structures had a width of <200 nm, a

value $\sim 1/6$ of the fundamental wavelength or $1/3$ the wavelength corresponding to the two-photon energy.

Comparison of 2PE and 1PE modes

To compare 2PE with 1PE, the excitation light sources were alternated in synchrony with the reciprocating scan direction allowing quasi-simultaneous imaging with two different lasers. The shear-force topography of a MitoTracker-labeled MCF7 cell is shown in Fig. 3 *A*, with the nucleus including two nucleoli at the bottom of the image. The fluorescence images recorded by 1PE of MitoTracker in the trace mode (*B*) and 2PE in the retrace mode (*C*) reveal the bright fluorescence of the mitochondria and the weaker fluorescence of the nucleoli. There was no detectable correlation between structures in the topographic and fluorescence images. The two fluorescence images were very similar except for the count rate. The power spectra of the 1PE and 2PE images showed no significant differences in spatial frequencies for either Fig. 3 (100×200 nm pixels) or other higher resolution images. Calculations of the mode shape in thin (200 nm diameter) optical fibers with a high refractive index difference between core and cladding for wavelengths in the range 488–633 nm show an invariant central mode

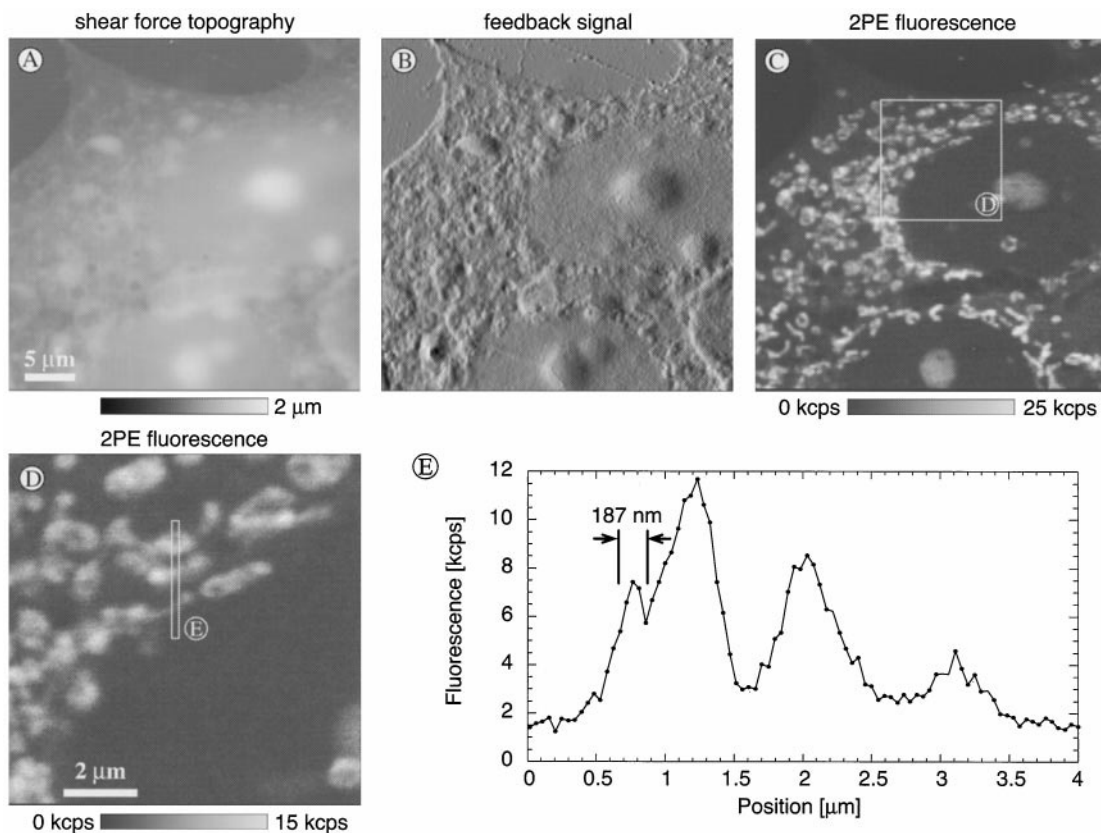


FIGURE 2 2PE SNOM image of MCF7 cells labeled with MitoTracker Orange. (*A*) Shear force topography, (*B*) topographic feedback (error) signal, (*C*) 2PE fluorescence signal. Scan parameters: 10 s/line, 128 lines, 256 points/line; excitation: 28 mW at 1064 nm. (*D*) Topography of the square zoom box marked in (*C*); scan parameters: 10 s/line, 256 lines, 256 points/line; excitation: 28 mW at 1064 nm. (*E*) Cross-sectional average line plot of the fluorescence from the area marked in (*D*).

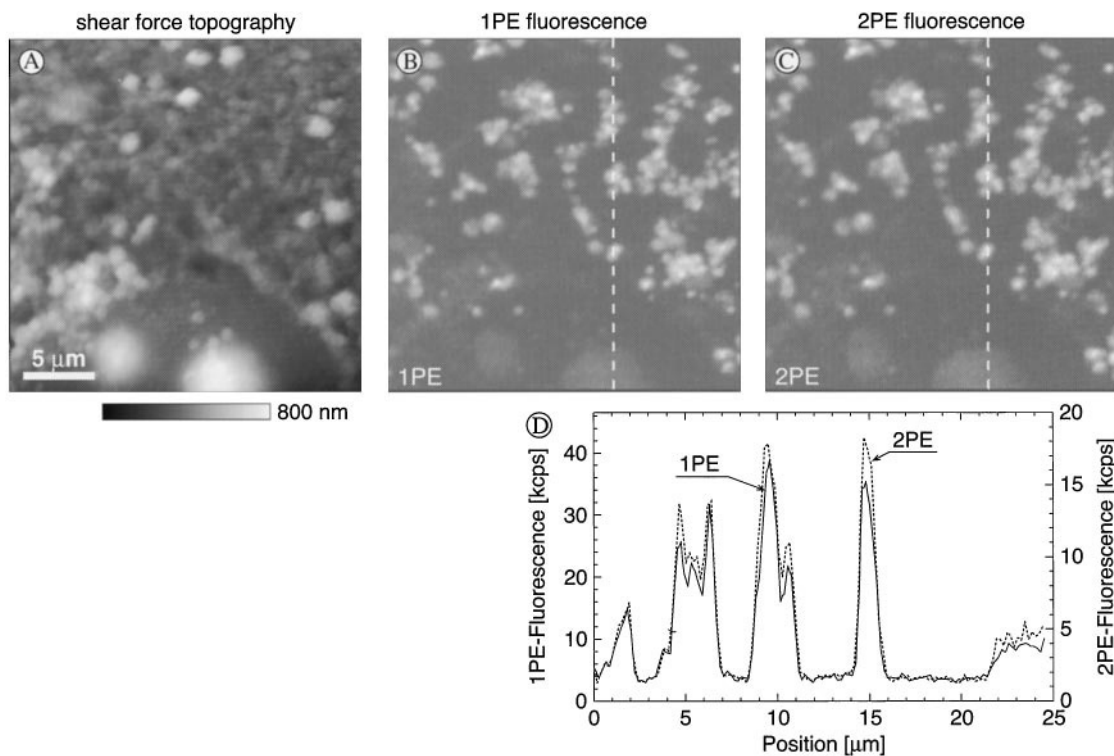


FIGURE 3 1PE and 2PE SNOM images of MCF7 cells. (A) shear force topography and (B) 1PE fluorescence (collected in trace mode) and (C) 2PE fluorescence signal (collected in retrace mode), of the MitoTracker Orange-labeled mitochondria. (D) Fluorescence intensity profiles along the dashed lines in B and C scaled for equal background levels. Scan parameters: 10 s/line, 128 lines, 256 points/line; excitation: 3.3 μ W at 532 nm (B) and 33 mW at 1064 nm (C).

structure accompanied by sidelobes whose prominence increases with wavelength (Kirsch, 1998). However, the quadratic dependence of 2PE should mitigate the effects of the sidelobes. The combination of all these effects leads to the conclusion that the lateral resolution in 1PE and 2PE should not differ significantly in our SNOM configuration.

To compare the signal-to-background ratios, two line traces along the dashed line in Fig. 3 B and Fig. 3 C were plotted in Fig. 3 D. Because of the lower relative background contribution to the 2PE signal, the signal-to-background ratio was 16% higher. The suppression in 2PE of fluorescence and Raman background from the optical fiber present in 1PE is a general advantage in both cw (Kirsch et al., 1998b) and pulsed multiphoton SNOM.

Simultaneous 2PE and 3PE imaging

Our previous experiments based on a cw laser source (Kirsch et al., 1998b) were restricted to 2PE of near-UV fluorophores. With the pulsed laser featured in this report we were able to simultaneously image near-UV and visible fluorophores with combined 2PE and 3PE. The multiparametric imaging of MCF 7 cells is featured in Fig. 4: (A) the shear-force topography signal, (B) 2PE fluorescence of MitoTracker, and (C) 3PE fluorescence of the BBI-342 DNA probe. The fluorescence from the two dyes was collected in separate channels. Perinuclear mitochondria appeared in the

2PE channel. The 3PE channel (C) recorded the staining of the nucleus with the DNA dye, thereby allowing the unambiguous assignment of the nuclear domain. The difference between the emission intensities was \sim 1:80; nonetheless, the 3PE signal was easily detectable. The dehydration and drying procedures led to a significant loss of BBI-342 binding, and consequently a reduction of the fluorescence signal. Mitochondria grouped around the nucleus were not detectable in the 3PE channel. Because of the large difference in the emission wavelengths of the two dyes, we were able to detect the two signals free of cross talk.

Specific protein bands in spread polytene chromosomes were also imaged using 2PE- and 3PE-SNOM. Fig. 5 shows (A) shear force topography, (B) 2PE fluorescence of the Cy3-conjugated antibodies, and (C) 3PE fluorescence of DAPI. The 3PE fluorescence of DAPI was lower than in previous cw 2PE studies (Kirsch et al., 1998b) but there was no evidence of photobleaching. Distinct, sharp sub-DNA bands labeled by the anti-PH antibody were revealed with a resolution significantly superior to that of the light microscope (Franke et al., 1992). The Cy3 2PE signal bleached relatively quickly between successive frames.

Fluorescence intensity curves

The dependence of the fluorescence intensity on excitation power was determined over a large range. In Fig. 6 A the tip

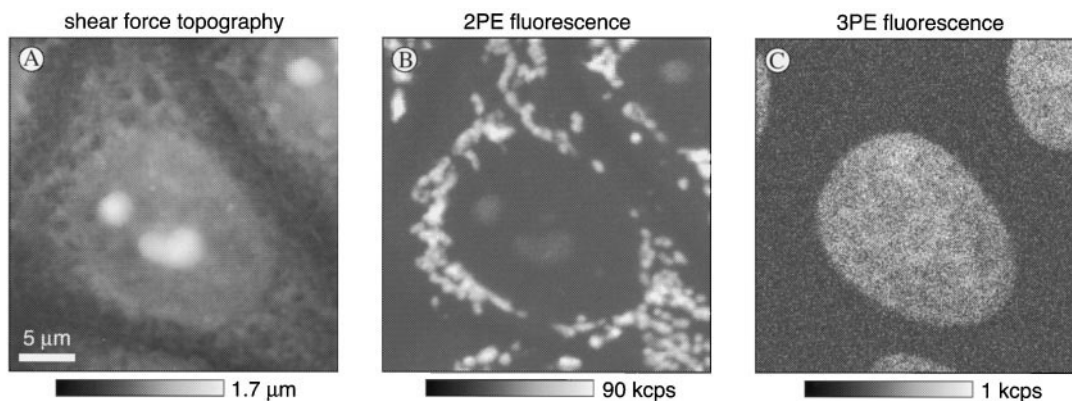


FIGURE 4 2PE and 3PE SNOM images of MCF7 cells. (A) Shear force topography, (B) 2PE fluorescence signal of the MitoTracker Orange-labeled mitochondria, and (C) 3PE fluorescence of the BBI-342-labeled nucleus. Scan parameters: 10 s/line, 128 lines, 256 points/line; excitation: 51 mW at 1064 nm.

was in shear force contact with a MitoTracker-labeled cell and located at a high fluorescence intensity area. In Fig. 6 B the target was a DAPI-labeled polytene chromosome. The excitation intensity I_n and fluorescence signal F_n were measured for each ND filter setting, and the measured dark count rate in the absence of laser excitation, F_0 , were subtracted. To the resulting data (I_n , $\Delta F_n = F_n - F_0$), we fit the function

$$\Delta F_n = a \cdot I_n^e \quad (1)$$

where a is the amplitude and e the exponent representing the order of the excitation. This functional form is commonly used in multiphoton studies. The value of e should be 2 for 2PE and 3 for three-photon absorption processes (Hell et al., 1996). The calculated exponents (Fig. 6) were very close to the expected theoretical values, indicating the absence of significant contributions of background linear effects (e.g., fiber fluorescence or excitation leakage into the detectors) to the signals.

We used different counting times (0.3 s for 2PE and 20 s for 3PE) for the different excitation modes to avoid photobleaching (in the 2PE case) and to increase the count rate and thus the signal-to-noise ratio (in the 3PE case). There was no detectable decrease in the 3PE signal during the measurements.

Dependence of signal intensity on axial displacement

One of the most important features of 2PE and 3PE in far-field laser scanning microscopy is the enhanced 3D resolution resulting from restriction of the excitation to a small focal volume. The corresponding effect in the shared-aperture SNOM is shown in Fig. 7. The axial dependence of the fluorescence intensity on the distance between the sample (a rhodamine B-doped PVA film) and the probe was recorded. The sample was excited with the pulsed laser at 1064 nm via 2PE (Fig. 7 A), whereas the frequency-doubled

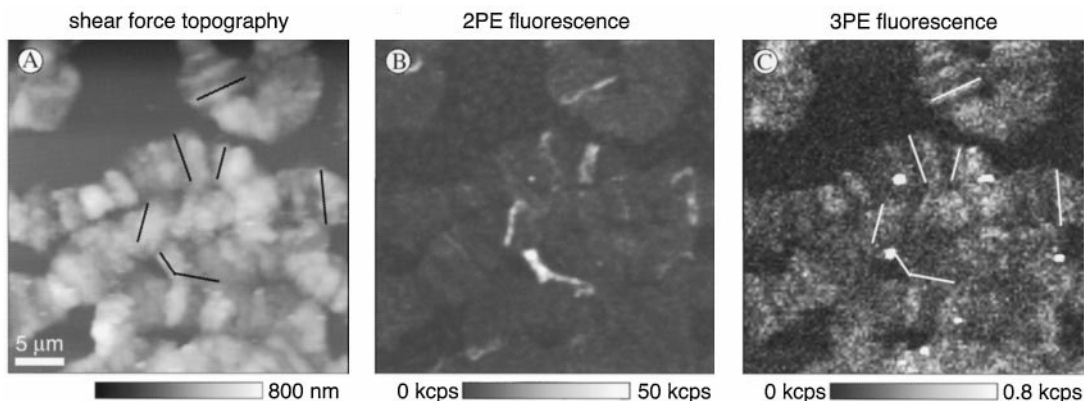


FIGURE 5 2PE and 3PE SNOM images of doubly labeled *Drosophila melanogaster* polytene chromosomes. (A) Shear force topography, (B) 2PE indirect immunofluorescence of the *Drosophila*-protein polyhomeotic (Cy3 fluorophore), and (C) 3PE fluorescence of DNA probe DAPI. Scan parameters: 10 s/line, 128 lines, 128 points/line; excitation: 48 mW at 1064 nm. The black lines in the topography image and white lines in (C) indicate bands of Cy3-labeled antibody-protein complexes with high 2PE fluorescence intensity.

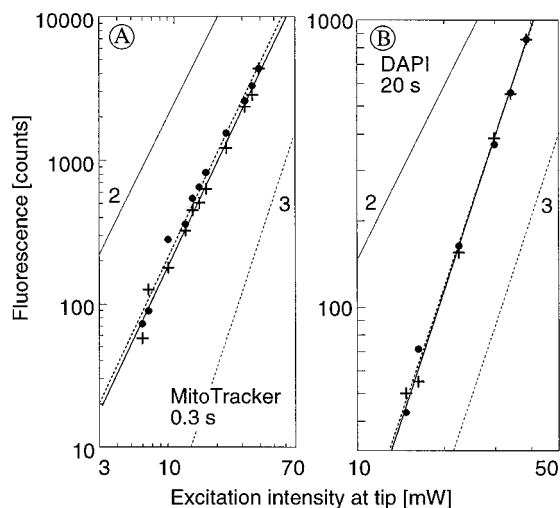


FIGURE 6 Power curves measured on (A) MitoTracker-labeled MCF7 cell and (B) polytene chromosome labeled with DAPI. The fluorescence intensity values at the fiber tip were measured by varying the excitation intensity using ND filters. Counting times: (A) 0.3 s, (B) 20 s. Data points for increasing excitation intensity (●) and linear fit to the logarithmic form of Eq. 1 (—); data for decreasing excitation intensity (+) and fit (· · · ·). As visual guides, each panel includes lines corresponding to ideal 2-photon (—) or 3-photon (· · · ·) processes flanking the data. Fits: 2PE-MitoTracker Orange, $\langle e \rangle = 2.10 \pm 0.11$; 3PE-DAPI, $\langle e \rangle = 2.94 \pm 0.07$.

Nd:YAG laser was used for 1PE of the same sample (Fig. 7 B). In Fig. 7 A only the first and sixth approach curves are shown; they exhibited clear photobleaching. In Figure 7 B, seven recorded approach curves are overlaid; there was no perceptible photobleaching in this case. As in our previous analysis (Kirsch et al., 1998b) a double exponential function

$$F_i = a_i \cdot \exp(-z/z_1) + b_i \cdot \exp(-z/z_2) + c_i \quad (2)$$

was fit to the data. F_i is the fluorescence signal for approach i , z_1 and z_2 are global decay lengths for the experiment, and a_i , b_i are the amplitudes, and c_i the offset, respectively, for approach i . A single exponential function failed to describe the data adequately. The curves resulting from the biexponential fits are shown as solid lines in Fig. 7.

The global decay lengths z_1 and z_2 are given in Table 1. Because of the biexponential nature of the decays, we characterized the axial dependence by the distance $z = H_i$, at which the fluorescence signal decreased to one-half of the value recorded with the probe in shear-force contact with the sample (Table 1). Before the determination of H_i the z -independent background c_i was subtracted. Due to bleaching in the 2PE case we used only the first three approach curves for determining a mean $\langle H_i \rangle$, which was smaller for 2PE than for 1PE. Thus, the thickness of the surface layer contributing to the optical signal in 2PE is smaller than in 1PE, constituting an additional benefit of multiphoton excitation.

Since we used the same sample for both experiments, the photobleaching behavior could be compared directly. Three effects were likely contributors to the increased photo-

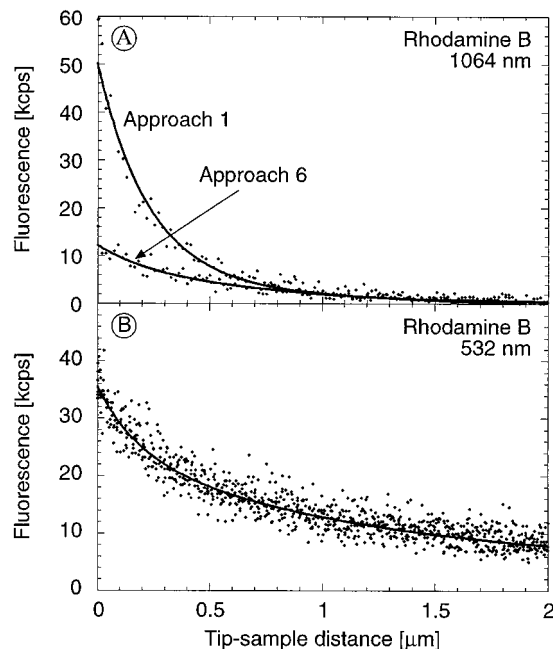


FIGURE 7 Axial fluorescence decay profile in 1PE and 2PE of rhodamine B-doped polyvinylalcohol (PVA) film. (A) Fluorescence signal excited by pulsed 1064-nm laser depicting the first and the sixth approaches; (B) fluorescence signal excited with cw 532-nm excitation. Solid lines are biexponential fits to the data; fit results are shown in Table 1. Excitation: 53 mW at 1064 nm (A) and 0.3 μ W at 532 nm (B). Counting time per data point, 4.1 ms.

bleaching in the 2PE case. First, the 60% higher initial intensity with 2PE suggested that the system was pumped to a greater degree of saturation than in 1PE. In addition, as seen from the approach curves, the thickness of the surface layer contributing to the fluorescence signal in 2PE was less than half of that in 1PE, implying the involvement of fewer fluorophores in the 2PE excitation volume. Finally, as noted by others (Eggeling et al., 1997; Sanchez et al., 1997; Lewis et al., 1998), an increased photobleaching for 2PE compared to 1PE may arise as a result of excited state reactions leading to other channels for irreversible photodestruction of the fluorophore. Specifically, for xanthene (rhodamine) dyes, Sanchez et al. (1997) suggested that enhanced 2PE photobleaching proceeds through absorption of the infrared excitation light by the first excited triplet state to higher triplet levels.

TABLE 1 Z-distance dependence for 1PE and 2PE

Excitation	z_1	z_2	$\langle H_i \rangle$
Single-photon (1PE)	180 nm	1164 nm	404 ± 62 nm
Two-photon (2PE)	227 nm	952 nm	178 ± 3 nm

z_1 and z_2 , decay lengths obtained from the simultaneous fit of the approach curves to a double exponential function (Eq. 2) with varying amplitudes for the individual approaches. $\langle H_i \rangle$, mean value between the probe and the sample surface at which the fluorescence signal dropped to one-half of the initial value at contact.

We note that the background contribution from fluorophores far away from the tip (Fig. 7, values for tip-sample displacement of $2\ \mu\text{m}$) was much smaller in the 2PE case than in 1PE. This effect is particularly important for thick samples, and can be considered analogous to the improved background characteristics of 2PE in the far-field, a further consequence of the restricted excitation volume.

Photobleaching measurements

The excitation distributions in 1PE and 2PE were characterized by the photobleaching of a rhodamine B-doped PVA film. Inasmuch as the lateral diffusion of the fluorophores was reduced drastically by the solid host matrix, the bleached patterns were stable over hours and even days. We photobleached lines in the film by repeatedly scanning (64 times) a single line with the same light intensity used to subsequently image the bleached pattern, using both 1PE at 532 nm (Fig. 8 A) and 2PE at 1064 nm (Fig. 8 B). Both lines were traced and imaged with the same fiber tip on different areas of the same sample. We intentionally over-illuminated the sample so as to emphasize any secondary features generated by light leakage from the fiber tip. In the 1PE case the bleached line was surrounded by a larger area exhibiting diffuse bleaching as well as weak secondary bleached lines (Fig. 8 A, inset). With 2PE the fluorescence of the film surrounding the line is uniform, and there were no visible effects of photobleaching in this area (Fig. 8 B, inset). The

consequences of the bleaching are seen more clearly in the averaged profiles normal to the bleached lines (Fig. 8, A and B). The secondary features generated by 1PE are readily evident in the profile shown in panel A. The shape of the central line photobleached by 1PE could be described by a combination of two overlapping Gaussian curves with full widths ($2\ \sigma$) of 0.5 and $1.9\ \mu\text{m}$. In contrast, 2PE was characterized by a single Gaussian of $0.9\ \mu\text{m}$ full width, with no effect of the excitation away from the central line.

The secondary photobleaching features were most likely results of coupling of the excitation light out from the conical part of the fiber several micrometers away from the surface. The 1064-nm excitation presumably also coupled out of the fiber, but because of the higher-order dependence of 2PE, the leakage intensity was apparently too weak to yield significant photobleaching. The relative width of the central line in the 2PE case was probably exaggerated because of the greater extent of photobleaching (Naber et al., 1996). Since the width of the central bleached lines are also likely influenced by many factors, including piezo drift during the repeated scanning, it is difficult to make a quantitative comparison between the 1PE and 2PE cases. However, a reduction or elimination of the secondary features resulting from lateral coupling of light out of the fiber was shown clearly for 2PE. This result has important implications for the microscopy of light-sensitive samples, imaging of which by conventional line-scan 1PE can involve photodamage in neighboring, as yet unscanned, regions. The effect is apparently suppressed, or at least diminished significantly, in 2PE-SNOM.

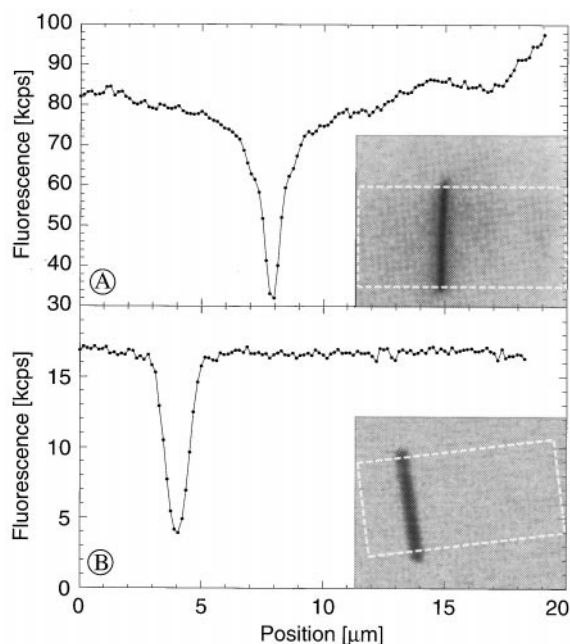


FIGURE 8 Fluorescence bleaching experiments on rhodamine B-doped PVA film. (A) 1PE bleached line after 64 scans (inset) and mean fluorescence intensity profile perpendicular to the bleached line. (B) 2PE bleached line (inset: note that this image was rotated by $\sim 7^\circ$ due to piezo drift) and mean fluorescence intensity profile perpendicular to bleached line. The dashed boxes indicate the areas over which the mean profiles were calculated. See text for experimental details.

CONCLUSIONS

We have demonstrated simultaneous two- and three-photon excitation in a shared aperture SNOM. This operational mode extends the accessible spectral range to the near-UV and also allows multicolor imaging of two different dyes free of cross talk. In addition, the background signal is significantly reduced, constituting one of the primary advantages of multiphoton excitation. The thickness of the surface layer contributing to the optical signal and the lateral extent of the excitation are also reduced significantly.

We thank S. W. Hell for providing the laser source for our measurements and for motivating discussions.

A. J. was supported by a long-term EMBO fellowship, and is also affiliated with the Department of Biophysics and Cell Biology, University Medical School of Debrecen, H-4012 Debrecen, Hungary. V. S. was supported by a long-term fellowship from the Human Frontiers Science Program Organisation.

REFERENCES

- Ashburner, M. 1989. Salivary gland chromosome squash technique: simple method. *In* *Drosophila, A Laboratory Manual*. Cold Spring Harbor Laboratory Press, Cold Spring Harbor, New York. 28–29.

- Bennett, B. D., T. L. Jetton, G. Ying, M. A. Magnuson, and D. W. Piston. 1996. Quantitative subcellular imaging of glucose metabolism within intact pancreatic islets. *J. Biol. Chem.* 271:3647–3651.
- Bewersdorf, J., and S. W. Hell. 1998. Picosecond pulsed two-photon imaging with a repetition rates of 200 and 400 MHz. *J. Microsc.* 191:28–38.
- Bielefeldt, H., I. Hörsch, G. Krausch, M. Lux-Steiner, J. Mlynek, and O. Marti. 1994. Reflection-scanning near-field optical microscopy and spectroscopy of opaque samples. *Appl. Phys. A: Solids Surf.* 59: 103–108.
- Braet, F., R. Dezanger, and E. Wisse. 1997. Drying cells for SEM, AFM and TEM by hexamethyldisilazane—a study on hepatic endothelial cells. *J. Microsc.* 186:84–87.
- Courjon, D., J. M. Vigoureaux, M. Spajer, K. Sarayedine, and S. Leblanc. 1990. External and internal-reflection near-field microscopy—experiments and results. *Appl. Opt.* 29:3734–3740.
- Curley, P. F., A. I. Ferguson, J. G. White, and W. B. Amos. 1992. Application of a femtosecond self-sustaining mode-locked Ti:sapphire laser to the field of laser scanning confocal microscopy. *Opt. Quantum Electron.* 24:851–859.
- Denk, W., D. W. Piston, and W. W. Webb. 1995. Two-photon molecular excitation in laser-scanning microscopy. In *Handbook of Biological Confocal Microscopy*. Plenum Press, New York. 445–458.
- Denk, W., J. H. Strickler, and W. W. Webb. 1990. Two-photon laser scanning fluorescence microscopy. *Science*. 248:73–76.
- Eggeling, C., L. Brand, and C. Seidel. 1997. Laser-induced fluorescence of coumarin derivatives in aqueous solution: photochemical aspects for single molecule detection. *Bioimaging*. 5:105–115.
- Franke, A., M. DeCamillis, D. Zink, N. Cheng, H. W. Brock, and R. Paro. 1992. *Polycomb* and *polyhomeotic* are constituents of a multimeric protein complex in chromatin of *Drosophila melanogaster*. *EMBO J.* 11:2941–2950.
- Gerdes, H. H., and C. Kaether. 1996. Green fluorescent protein: applications in cell biology. *FEBS Lett.* 389:44–47.
- Göppert-Mayer, M. 1931. Über Elementarakte mit zwei Quantensprüngen. *Annalen der Physik*. 9:273–295.
- Gryczynski, I., H. Malak, and J. R. Lakowicz. 1995. Three-photon induced fluorescence of 2,5-diphenyloxazole with a femtosecond Ti:sapphire laser. *Chem. Phys. Lett.* 245:30–35.
- Hänninen, P. E., E. Soini, and S. W. Hell. 1994. Continuous wave excitation two-photon fluorescence microscopy. *J. Microsc.* 176:222–225.
- Haugland, R. P. 1996. *Handbook of Fluorescent Probes and Research Chemicals*. Molecular Probes, Eugene, OR.
- Hell, S. W., K. Bahlmann, M. Schrader, A. Soini, H. Malak, I. Gryczynski, and J. R. Lakowicz. 1996. Three-photon excitation in fluorescence microscopy. *J. Biomed. Opt.* 1:71–74.
- Hell, S. W., M. Booth, S. Wilms, C. M. Schmetter, A. K. Kirsch, D. J. Arndt-Jovin, and T. M. Jovin. 1998. Two-photon near- and far-field fluorescence microscopy with continuous-wave excitation. *Opt. Lett.* 23:1238–1240.
- Kirsch, A. K. 1998. *Biologische Anwendung der Fluoreszenz-Nahfeldmikroskopie*. Ph.D. Thesis. University of Konstanz, Germany. Cuvillier Verlag, Göttingen, Germany.
- Kirsch, A. K., C. K. Meyer, H. Huesmann, D. Möbius, and T. M. Jovin. 1998a. Fluorescence SNOM of domain structures of LB films containing electron transfer systems. *Ultramicroscopy*. 71:295–302.
- Kirsch, A., C. Meyer, and T. M. Jovin. 1996. Integration of scanning probe microscopes with optical techniques. In *NATO Advanced Research Workshop: Analytical Use of Fluorescent Probes in Oncology*, Miami, FL. Plenum Press, New York. 317–323.
- Kirsch, A. K., C. K. Meyer, and T. M. Jovin. 1997. Shear force imaging of DNA in a near-field scanning optical microscope (NSOM). *J. Microsc.* 185:396–401.
- Kirsch, A. K., V. Subramaniam, G. Striker, C. Schmetter, D. J. Arndt-Jovin, and T. M. Jovin. 1998b. Continuous wave two-photon scanning near-field optical microscopy. *Biophys. J.* 75:1513–1521.
- König, K., U. Simon, and K. J. Halhuber. 1996. 3D resolved two-photon fluorescence microscopy of living cells using a modified confocal laser scanning microscope. *Cell. Mol. Biol.* 42:1181–1194.
- Lewis, M. K., P. Wolanin, A. Gafni, and D. G. Steel. 1998. Near-field scanning optical microscopy of single molecules by femtosecond two-photon excitation. *Opt. Lett.* 23:1111–1113.
- Maiti, S., J. B. Shear, W. R. Zipfel, R. W. Williams, and W. W. Webb. 1997. Measuring serotonin distributions in live cells with three-photon excitation. *Science*. 275:530–532.
- Naber, A., H. Kock, and H. Fuchs. 1996. High resolution lithography with near-field optical microscopy. *Scanning*. 18:567–571.
- Paesler, M., and N. F. van Hulst, editors. 1995. *Near-field optics and related techniques*. In *Ultramicroscopy*. Elsevier, Amsterdam. 61.
- Pietrasanta, L. I., A. Schaper, and T. M. Jovin. 1994. Imaging subcellular structures of rat mammary carcinoma cells by scanning force microscopy. *J. Cell Sci.* 107:2427–2437.
- Potter, S. M., C. M. Wang, P. A. Garrity, and S. E. Fraser. 1996. Intravital imaging of green fluorescent protein using two-photon laser-scanning microscopy. *Gene*. 173:25–31.
- Sanchez, E. J., L. Novotny, G. R. Holtom, and X. S. Xie. 1997. Toom-temperature fluorescence imaging and spectroscopy of single molecules by two-photon excitation. *J. Phys. Chem. A*. 101:7019–7023.
- Schrader, M., K. Bahlmann, and S. W. Hell. 1997. Three-photon-excitation microscopy: theory, experiment and applications. *Optik*. 104:116–124.
- Summers, R. G., D. W. Piston, K. M. Harris, and J. B. Morrill. 1996. The orientation of first cleavage in the sea urchin embryo, *Lytechinus variegatus*, does not specify the axes of bilateral symmetry. *Dev. Biol.* 175:177–183.
- Szmazinski, H., I. Gryczynski, and J. R. Lakowicz. 1996. Three-photon induced fluorescence of the calcium probe indo-1. *Biophys. J.* 70: 547–555.
- Wokosin, D. L., V. Centonze, J. G. White, D. Armstrong, G. Robertson, and A. I. Ferguson. 1996. All-solid-state ultrafast lasers facilitate multiphoton excitation fluorescence imaging. *IEEE JSTQE*. 2:1051–1065.
- Xu, C., and W. W. Webb. 1996. Measurement of two-photon excitation cross sections of molecular fluorophores with data from 690 to 1050 nm. *J. Opt. Soc. Am. B*. 13:481–491.
- Xu, C., W. Zipfel, J. B. Shear, R. M. Williams, and W. W. Webb. 1996. Multiphoton fluorescence excitation: new spectral windows for biological nonlinear microscopy. *Proc. Natl. Acad. Sci. USA*. 93:10763–10768.